NANO LETTERS

2008
Vol. 8, No. 5
1363-1367

Exciton Energy Transfer in Pairs of Single-Walled Carbon Nanotubes

Huihong Qian,[†] Carsten Georgi,[†] Neil Anderson,[‡] Alexander A. Green,[§] Mark C. Hersam,[§] Lukas Novotny,[‡] and Achim Hartschuh*[,†]

Department Chemie and Biochemie and CeNS, Ludwig-Maximilians-Universität München, 81377 München, Germany, University of Rochester, The Institute of Optics, Rochester, New York 14627, Department of Materials Science and Engineering, Department of Chemistry, Northwestern University, Evanston, Illinois 60208-3108

Received January 7, 2008; Revised Manuscript Received February 26, 2008

ABSTRACT

We studied the exciton energy transfer in pairs of semiconducting nanotubes using high-resolution optical microscopy and spectroscopy on the nanoscale. Photoluminescence from large band gap nanotubes within bundles is observed with spatially varying intensities due to distance-dependent internanotube transfer. The range of efficient energy transfer is found to be limited to a few nanometers because of competing fast nonradiative relaxation responsible for low photoluminescence quantum yield.

Single-walled carbon nanotubes (SWNTs) feature unique electronic properties, making them ideal candidates for ultrahigh density devices in electronics, photonics, and optoelectronics.[1–3] At nanoscale distances, energy transfer from large to small band gap nanotubes is expected to occur, facilitating novel architectures including crossbars and 3D arrays but also imposing design restrictions. Photoluminescence (PL) in semiconducting nanotubes results from exciton recombination[4–6] and is found to be quenched in bundles.[7–10] Very recently, resonant exciton energy transfer between semiconducting nanotubes has been observed for SWNTs in micelles suspensions for the first time and was explained by near-field coupling corresponding to fluorescence resonance energy transfer (FRET) well-known for molecular systems.[11] In ref 12, spectroscopic signatures of internanotube transfer were observed, and it was suggested that efficient coupling results from carrier migration requiring direct physical contact. In ensemble measurements, however, the identification of donor and acceptor spectral signatures is complicated by overlapping contributions from different nanotube species, including phonon-assisted absorption and possible emission from lower lying defect-associated states.[13–15] Up to now, the range of exciton transfer and its efficiencies are unknown.

We used tip-enhanced near-field optical microscopy (TENOM[16–18]) as a tool to visualize energy transfer in pairs of semiconducting nanotubes forming bundles and crossings on a nanometer length scale. Near-field PL and topography images of a single nanotube bundle reveal the presence of two semiconducting nanotubes with different chiralities having an internanotube spacing ranging from 1 to 4 nm. Photoluminescence from large band gap nanotubes was observed with unexpectedly high intensities although varying spatially along the nanotubes due to distance-dependent internanotube energy transfer. Efficient transfer is found to be limited to a few nanometers because of competing fast nonradiative relaxation and can be explained in terms of electromagnetic near-field coupling. From the experimental data, we estimate transfer efficiencies and time scales.

The setup used for near-field optical microscopy and spectroscopy is based on an inverted confocal optical microscope that is combined with a scan head for shear-force detection providing tip–sample distance control.[16–18] The signal is detected either by a combination of a spectrograph and a cooled charged coupled device (CCD) or by a single-photon counting avalanche photodiode (APD) after spectral filtering. Both detectors are silicon-based, limiting our spectral detection range in the near-infrared to about 1050 nm. A near-field optical image is established by raster scanning the sample and simultaneously recording topographic and optical signals. CoMoCAT SWNTs were sorted by using discriminating surfactants and wrapped by DNA after sorting. Density gradient ultracentrifugation isolates nanotubes with a narrow chirality distribution.[19–21] Chirality-enriched materials increase the probability for observing two interacting semiconducting nanotubes with similar excited-state energies, supporting resonant energy transfer and

* Corresponding author. E-mail: Achim.hartschuh@cup.unimuenchen.de.
[†] Department Chemie and Biochemie and CeNS, Ludwig-Maximilians-Universität München.
[‡] University of Rochester, The Institute of Optics.
[§] Department of Materials Science and Engineering, Department of Chemistry, Northwestern University.

10.1021/nl080048r CCC: $40.75
Published on Web 03/27/2008

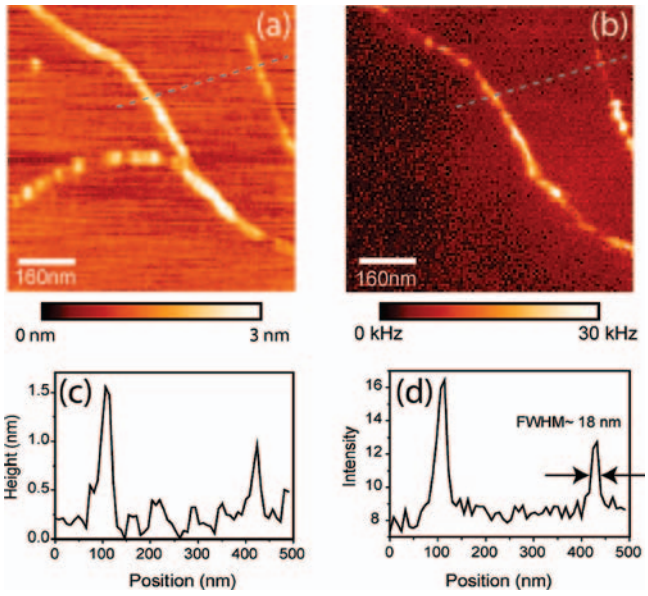

Figure 1. Simultaneously recorded topography (a) and near-field PL image (b) of DNA-wrapped single-walled carbon nanotubes on mica. The scan area is 800 × 800 nm^2. The PL image was formed by detecting all emission between 860 and 1050 nm upon laser excitation at 632.8 nm using 5 μW. (c,d) Cross sections taken along the dashed lines in (a) and (b), respectively. The height of the nanotube structure extending from the upper left to the lower right corresponds to what is expected for single DNA-wrapped nanotubes and varies from 1.5 to 2.5 nm. The optical resolution of ≈18 nm is derived from the fwhm of the peaks in the cross section in (d).

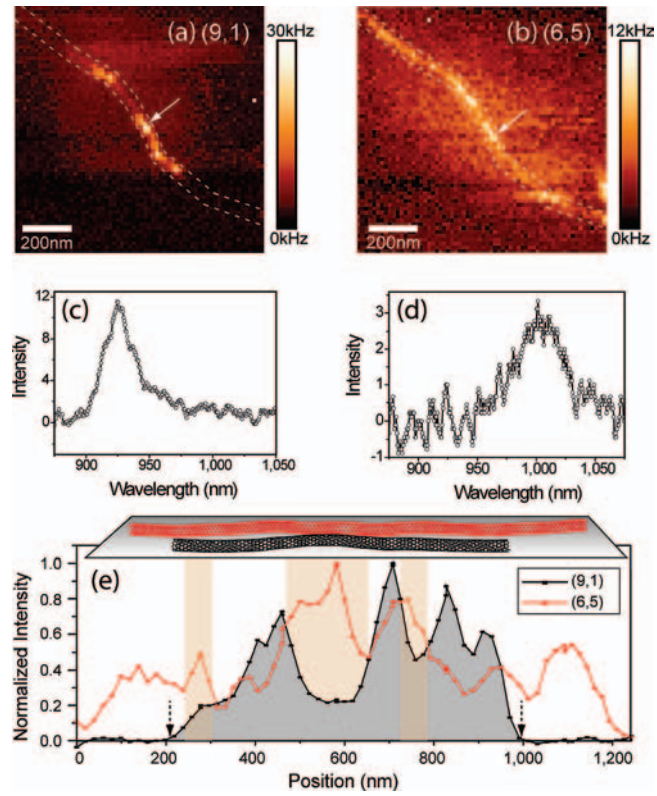

Figure 2. Near-field PL images with 64 × 64 pixel of the DNA-wrapped single-walled carbon nanotubes seen in Figure 1 obtained by measuring spectra at each pixel. (a) and (b) represent the integrated intensities within selected spectral windows ranging from 910 to 940 nm for (a) covering the emission of (9,1) nanotubes and from 990 to 1020 nm for (b) covering the (6,5) emission. Evidently, the nanotube structure seen in Figure 1 is a nanotube bundle composed of two nanotubes with different chiralities. The chirality assignment is based on the emission spectra detected at the positions marked with the white arrows shown in (c) and (d) that exhibit the characteristic energies of (9,1) and (6,5) nanotubes, respectively. The scan area is 1 × 1 μm^2. Laser excitation at 632.8 nm with 100 μW and an integration time of 400 ms per spectrum were used. (e) presents intensity profiles taken along the (9,1) (black line) and the (6,5) nanotube (red line) summed between the two dashed lines in (a) and (b), respectively. The two dashed arrows mark beginning and end of the (9,1) nanotube determined from the simultaneously detected G-band Raman signal (not shown).

facilitating their optical detection. The sample was made by spin-coating the nanotube solution on a freshly cleaved thin layer of mica glued on a glass cover slide. The mica layer was positively charged by Mg ions to increase the surface adhesion of the negatively charged DNA site of the hybrid.

Figure 1 illustrates the topography (a) and the simultaneously recorded near-field PL image (b) of DNA-wrapped nanotubes. The PL image represents the intensity detected in the spectral range from 860 to 1050 nm and features a spatial resolution of 18 nm. The sharp and intense PL spots of the nanotube on the right indicate the presence of highly localized excited states that could be formed by lower lying states related to charged defects or environmental perturbations.[16] In contrast, the nanotube structure extending from the upper left to the lower right exhibits rather uniform and extended PL intensity, a typical observation for DNA-wrapped nanotubes and nanotubes in SDS micelles.[16] The nanotube oriented horizontally extending from the left into the center of the topographic image is not visible in the PL image and is therefore either metallic or its luminescence energy is outside of our detection range.

In the following, we focus on the nanotube structure extending from the upper left to the lower right that is clearly visible in both images. The topographic height of the structure is around 1.5−2.5 nm (Figure 1a,c), a value expected for single DNA-wrapped nanotubes.[22] However, on the basis of the topographic data, it will be extremely difficult to distinguish single nanotubes from thin bundles. The uniform height of the structure and the absence of larger adherent particles that could modify the tip−nanotube distance and thus affect the signal enhancement provided by the tip[17,18,23] allows us to directly compare intensities at different nanotube sections and to attribute changes to nanotube properties.

Figure 2 presents PL images derived from spectra taken at each pixel of the sample area from Figure 1. After splitting the emission into two selected spectral windows, the structure extending from the upper left to the lower right in parts a and b of Figure 1 is found to be a thin bundle containing a (9,1) and a (6,5) nanotube, as evidenced by the emission energies around 925 nm and around 1000 nm, respectively (Figure 2c,d). The red-shift compared to the 912 nm emission energy reported for the (9,1) nanotube and the 975 nm for (6,5)[24] results from DNA-wrapping.[25] In ref 26, bundling was found to cause large red-shifts of elastic scattering signals for thicker nanotubes by up to 47 meV. While we observed

smaller emission energy fluctuations by 12 and 16 meV in the spectra along the (6,5) and the (9,1) nanotube in Figure 2, respectively, such shifts can also be explained by nonuniform DNA-wrapping as found for single DNA-wrapped nanotubes.[27]

Emission from the (9,1) nanotube (Figure 2a) occurs in four bright segments, while emission from the (6,5) nanotube (Figure 2b) is more extended for about 1 μm. This can also be seen in the intensity profiles shown in Figure 2e taken along the two dashed lines in Figure 2a,b. The four bright segments in the cross section of the (9,1) nanotube feature lengths between 80 and 150 nm. As four independent short (9,1) nanotubes attached regularly along the (6,5) nanotube would be very unlikely and because the PL of the (9,1) does not disappear completely in between the bright segments, it is evident that we observe a bundle formed by a (9,1) and a (6,5) nanotube. Moreover, characteristic G-band Raman scattering was observed from the (9,1) nanotube that is resonantly enhanced at $E_{laser} = E_{22}(9,1) + h\omega_G$ extending along the detected PL spots marked by dashed arrows in Figure 2e.[24,28] Raman scattering from the (6,5) nanotube is not detected because of weak electronic resonances and low excitation power.

Remarkably, the PL of the (6,5) nanotube is found to be stronger when the PL of the (9,1) nanotube decreases, seen for example in the center of the cross sections between 460 and 640 nm and around 280 and 740 nm. Strong PL of the (9,1) nanotube on the other hand occurs in sections where (6,5) emission is weaker, e.g., at 420 nm and between 780 and 920 nm. We attribute this anticorrelation of the PL intensities to energy transfer from the large band gap (9,1) nanotube to the small band gap (6,5) nanotube as expected in bundles. However, the fact that PL from (9,1) is still detectable even within the bundle clearly shows that the efficiency of the energy transfer is limited. Spatial variations of the transfer efficiency can be understood in terms of varying internanotube distances. The finite length of DNA segments and resulting partial DNA wrapping could allow for different nanotube−nanotube spacing. In some regions, the PL intensity of the (9,1) nanotube increases slightly following that of the (6,5) nanotube, e.g., between 330 and 400 nm and 650 and 700 nm, which might be caused by local defects or environmental perturbations.

Besides several cases for energetic coupling of nanotubes within bundles, we observed indications for transfer in nanotube intersections. An example is presented in Figure 3a−c. On the basis of their emission energies (spectrum 1 and 2 in Figure 3d), the nanotubes crossing in the center of the image are identified as (8,3) and (6,5), respectively. At the intersection however, only the PL of the small band gap nanotube (6,5) is observed (spectrum 3 in Figure 3d). The topographic height at the crossing point is about 3 nm (data not shown), indicating that the maximum wall-to-wall distance between the two intersecting nanotubes is around 1.5 nm based on nanotube diameters of 0.75 nm. The reduced intensity of the large band gap nanotube (8,3) at the intersection implies that energy transfer occurs in the present configuration for wall-to-wall distances between 0 and 1.5

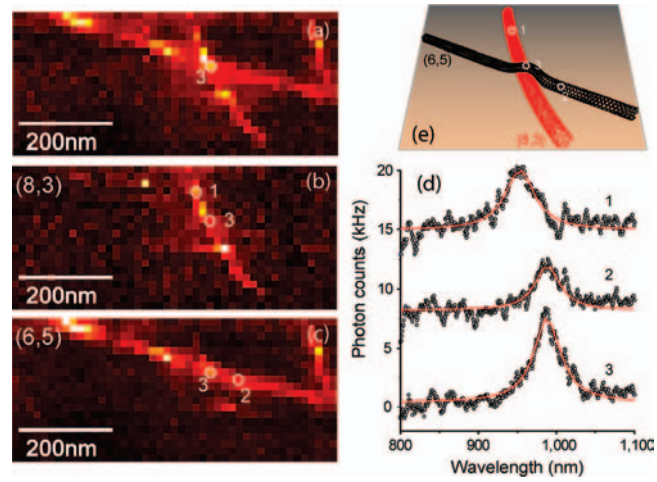

Figure 3. Near-field PL image of two intersecting nanotubes obtained by measuring spectra at each pixel representing the integrated intensity within selected spectral windows. (a) Total intensity. The intensity integrated from 915 to 945 nm is shown in (b) and from 970 to 1010 nm in (c). (d) Spectra taken at the pixels marked by white circles and numbers 1–3 in (a), (b), and (c). (e) Simplified schematic of the intersecting nanotubes.

nm. Notably, emission from the (8,3) nanotube is found to recover within a few nanometers distance to the intersection (Figure 3b), indicating that the range of efficient transfer is limited in agreement with our findings for the nanotube bundle in Figure 2.

On the basis of the image data presented in Figure 2, we now estimate the efficiency, the range, and the time constant of energy transfer. As the nanotubes in Figure 1a can not be distinguished by our topographic data, optical information can be used to determine the position of two spectrally isolated emitters with nanometer accuracy far below the resolution limit of the experiment.[29,30] Cross sections perpendicular to the nanotubes were taken at different locations in (Figure 2a,b) and were fit with Gaussian line shape functions to determine the in-plane position with maximum intensity for the two spectral windows (data not shown). Center-to-center distances ranging from $d = 1$ to 4 nm were found between the maxima of the two nanotubes in corresponding cross sections. For each distance, we determined the transfer efficiency $E(d) = 1 - I(d)/I_0$ using the measured intensities $I(d)$ and of the (9,1) nanotube. The data points (Figure 4b) reveal a very fast decay and support our assignment of the PL intensity variations to variations of distance-dependent energy transfer.

To derive the energy transfer rate k_{ET}, the ratio of the PL intensities n is expressed as the ratio of the PL quantum yields Q_{PL} with and $Q_{PL,0}$ without energy transfer

$$n = I/I_0 = Q_{PL}/Q_{PL,0} = \frac{k_r + k_{nr}}{k_r + k_{nr} + k_{ET}} \qquad (1)$$

Here k_r and k_{nr} and denote the radiative and the nonradiative rate in the presence of the metal tip. The total decay rate of individual DNA-wrapped (9,1) nanotubes in the absence of a metal tip at room temperature is about $k = k_r + k_{nr} \approx (8\ \text{ps})^{-1}$ being dominated by k_{nr}.[31] In the case of tip-enhancement, this value will represent a lower limit

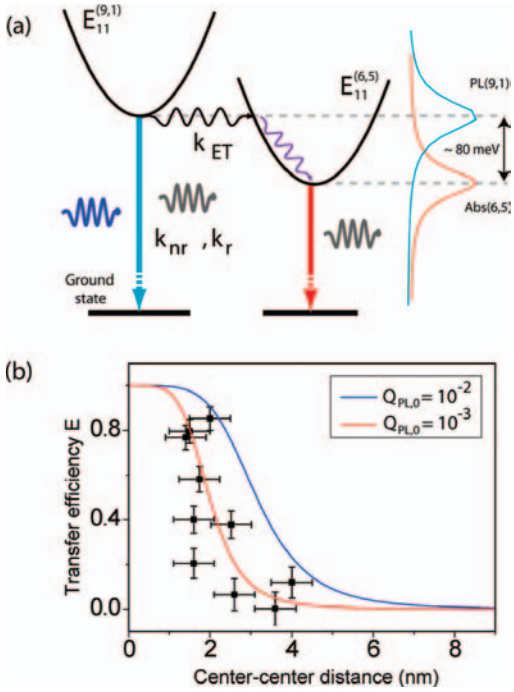

Figure 4. (a) Energy level scheme of resonant transfer in a single donor–acceptor pair formed by a (9,1) and a (6,5) nanotube. (b) Distance dependence of the energy transfer efficiency $E(d)= 1 - I(d)/I_0$ for a single (9,1)/(6,5) pair determined from the data shown in Figure 2. The internanotube distance was determined from the center of Gaussian line shape functions fitted to cross sections taken at different positions along the nanotube bundle in the PL images. The solid lines are calculated Förster energy transfer efficiencies accounting for a PL quantum yield of $Q_{PL.0} = 10^{-2}$ (blue line) and $Q_{PL.0} = 10^{-3}$ (red line), respectively (Supporting Information).

because the tip is expected to increase both radiative and nonradiative decay rates.[16,23] As a result, the maximum transfer rate $k_{ET} \approx k(1 - n)/n$ observed in our measurements is about 0.5 ps^{-1}.

Using our findings for the transfer range and the time scales, we can discuss contributions from different possible transfer mechanisms. Electron tunneling observed for nanotube intersections and between the constituents of multiwalled nanotubes requires overlapping wave functions and will be short ranged on a subnanometer scale.[32] Förster-type transfer efficiencies can be calculated for molecular systems as a function of the dipole–dipole distance. For extended quasi-one-dimensional nanotubes the near-field radiation pattern and thus the effective transfer rates are expected to be different.[33] Here we calculate the Förster transfer efficiency as a first estimate for the contribution of near-field interactions. The transfer efficiencies considering $Q_{PL.0}$ formed by integrating along the z-axis of the accepting nanotube, $E(d) = 1/(1 + (Q_{PL.0} \int_{-\infty}^{\infty} (R_0/R)^6 \, dz)^{-1})$, are shown in Figure 4b together with the experimentally determined values from Figure 2 (Supporting Information). Good agreement can be seen for a quantum yield of $Q_{PL.0} = 10^{-3}$, a typical value discussed for nanotubes on substrates. Exciton transfer clearly depends very sensitively on the nanotube−nanotube distance and is limited to only few nanometers because of competing fast nonradiative relaxation processes leading to low $Q_{PL.0}$.

According to Förster theory, the energy transfer efficiency depends on the spectral overlap of emission and absorption bands and will therefore be controlled by the chirality tuple $(n,m)_{donor}/(n,m)_{acceptor}$ of a particular donor–acceptor nanotube pair. The present observation of efficient transfer for the (9,1)/(6,5) nanotube pair spaced by few nanometers and having a spectral shift of ~80 meV between emission and absorption maxima supports the discussion in ref 11 on the energy transfer in bundles. In addition, phonon-assisted absorption of the accepting nanotube is likely to increase spectral overlap.[15] While in the case of the (8,3)/(6,5) nanotube pair in Figure 3, the overlap will be large due to a small spectral shift of ~30 meV, the particular cross configuration will reduce transfer by decreasing the orientational factor κ (Supporting Information). In general, maximum transfer efficiency and range are expected for parallel nanotubes within bundles.

In summary, we observed exciton energy transfer in pairs of semiconducting nanotubes using high-resolution optical microscopy and spectroscopy. Transfer efficiencies between two nanotubes were quantified for different internanotube distances and explained by Förster-type electromagnetic near-field coupling. The range of efficient transfer is found to be limited to a few nanometers because of competing fast nonradiative relaxation responsible for low photoluminescence quantum yield. For highly luminescent materials, on the other hand, transfer is predicted to be long-ranged and needs to be considered in the design of integrated exciton-based devices.

Acknowledgment. The authors wish to acknowledge P. Gucciardi and N. Hartmann for experimental support. This work was funded by the National Science Foundation (grant CHE-0454704), U.S. Department of Energy (grant DE-FG02-05ER46207), the Deutsche Forschungsgemeinschaft (DFG-HA4405/3-1), and the Nanosystems Initiative Munich (NIM). Support from an Alfred P. Sloan Research Fellowship (M.C.H.) and a Natural Sciences and Engineering Research Council of Canada Fellowship (A.A.G.) are gratefully acknowledged. This work was also funded by the U.S. National Science Foundation under award nos. EEC-0647560 and DMR-0706067.

Supporting Information Available: Information supporting distance dependence of the energy transfer efficiency for a single (9,1)/(6,5) pair (Figure 4b), experimentally determined values from Figure 2, and the orientational factor influencing the (8,3)/(6,5) nanotube pair in Figure 3. This material is available free of charge via the Internet at http://pubs.acs.org.

References

(1) Jorio, A., Dresselhaus, M. S., Dresselhaus, G., Eds. *Carbon Nanotubes*; Topics in Applied Physics, Volume 111; Springer: Berlin/Heidelberg, 2008.
(2) Lu, W.; Lieber, C. M. *Nat. Mater.* **2007**, *6*, 841–850.
(3) Avouris, P.; Chen, J. *Mater. Today* **2006**, *9*, 46–54.
(4) Wang, F.; Dukovic, G.; Brus, L. E.; Heinz, T. F. *Science* **2005**, *308*, 838–841.
(5) Maultzsch, J.; Pomraenke, R.; Reich, S.; Chang, E.; Prezzi, D.; Ruini, A.; Molinari, E.; Strano, M. S.; Thomsen, C.; Lienau, C. *Phys. Rev. B* **2005**, *72*, 241402(R).

(6) Hagen, A.; Steiner, M.; Raschke, M. B.; Lienau, C.; Hertel, T.; Qian, H.; Meixner, A. J.; Hartschuh, A. *Phys. Rev. Lett.* **2005**, *95*, 197401–197404.
(7) Hertel, T.; Fasel, R.; Moos, G. *Appl. Phys. A: Mater. Sci. Process.* **2002**, *75*, 449–465.
(8) O'Connell, M. J.; Bachilo, S. M.; Huffman, C. B.; Moore, V. C.; Strano, M. S.; Haroz, E. H.; Rialon, K. L.; Boul, P. J.; Noon, W. H.; Kittrell, C.; Ma, J.; Hauge, R. H.; Weisman, R. B.; Smalley, R. *Science* **2002**, *297*, 593–596.
(9) Reich, S.; Dworzak, M.; Hoffmann, A.; Thomsen, C.; Strano, M. S. *Phys. Rev. B* **2005**, *71*, 033402.
(10) Crochet, J.; Clemens, M.; Hertel, T. *J. Am. Chem. Soc.* **2007**, *129*, 8058–8059.
(11) Tan, P. H.; Rozhin, A. G.; Hu, P.; Scardaci, V.; Milne, W. I.; Ferrari, A. C. *Phys. Rev. Lett.* **2007**, *99*, 137402–137404.
(12) Torrens, O. N.; Milkie, D. E.; Kikkawa, J. M. *Nano Lett.* **2006**, *6*, 2864–2867.
(13) McDonald, T. J.; Blackburn, J. L.; Metzger, W. K.; Rumbles, G.; Heben, M. J. *J. Phys. Chem. C* **2007**, *111*, 17894–17900.
(14) Kiowski, O.; Arnold, K.; Lebedkin, S.; Hennrich, F.; Kappes, M. M. *Phys. Rev. Lett.* **2007**, *99*, 237402–4.
(15) Plentz, F.; Ribeiro, H. B.; Jorio, A.; Strano, M. S.; Pimenta, M. A. *Phys. Rev. Lett.* **2005**, *95*, 247401–4.
(16) Hartschuh, A.; Qian, H.; Meixner, A. J.; Anderson, N.; Novotny, L. *Nano Lett.* **2005**, *5*, 2310–2313.
(17) Hartschuh, A.; Sánchez, E. J.; Xie, X. S.; Novotny, L. *Phys. Rev. Lett.* **2003**, *90*, 095503–095506.
(18) Kawata, S., Shalaev, V. M., Eds. *Tip Enhancement*; Advances in Nano-Optics and Nano-Photonics; Elsevier: Amsterdam, 2007.
(19) Arnold, M. S.; Green, A. A.; Hulvat, J. F.; Stupp, S. I.; Hersam, M. C. *Nat. Nanotechnol.* **2006**, *1*, 60–65.
(20) Arnold, M. S.; Stupp, S. I.; Hersam, M. C. *Nano Lett.* **2005**, *5*, 713–718.
(21) Green, A. A.; Hersam, M. C. *Mater. Today* **2007**, *10*, 59–60.
(22) Jin, H.; Jeng, E. S.; Heller, D. A.; Jena, P. V.; Kirmse, R.; Langowski, J.; Strano, M. S. *Macromolecules* **2007**, *40*, 6731–6739.
(23) Anger, P.; Bharadwaj, P.; Novotny, L. *Phys. Rev. Lett.* **2006**, *96*, 113002–113004.
(24) Bachilo, S. M.; Strano, M. S.; Kittrell, C.; Hauge, R. H.; Smalley, R.; Weisman, R. B. *Science* **2002**, *298*, 2361–2366.
(25) Fagan, J. A.; Simpson, J. R.; Bauer, B. J.; De Paoli Lacerda, S. H.; Becker, M. L.; Chun, J.; Migler, K. B.; Hight Walker, A. R.; Hobbie, E. K. *J. Am. Chem. Soc.* **2007**, *129*, 10607–10612.
(26) Wang, F.; Sfeir, M. Y.; Huang, L.; Huang, H. X. M.; Wu, Y.; Kim, J.; Hone, J.; O'Brien, S.; Louis, E.; Brus, L. E.; Heinz, T. F. *Phys. Rev. Lett.* **2006**, *96*, 167401–4.
(27) Qian, H.; Georgi, C.; Gokus, T.; Hartmann, N.; Green, A. A.; Hersam, M. C.; Novotny, L.; Hartschuh, A. to be submitted for publication.
(28) Dresselhaus, M. S.; Dresselhaus, G.; Saito, R.; Jorio, A. *Phys. Rep.* **2006**, *409*, 47–99.
(29) Heinlein, T.; Biebricher, A.; Schlüter, P.; Roth, C. M.; Herten, D.-P.; Wolfrum, J.; Heilemann, M.; Müller, C.; Tinnefeld, P.; Sauer, M. *ChemPhysChem.* **2005**, *6*, 949–955.
(30) Yildiz, A.; Tomishige, M.; Vale, R. D.; Selvin, P. R. *Science* **2004**, *303*, 676–678.
(31) Hartschuh, A.; Gokus, T.; Harutyunyan, H. *Abstract submitted to Nanotube 07 conference* 2007.
(32) Bourlon, B.; Miko, C.; Forro, L.; Glattli, D. C.; Bachtold, A. *Phys. Rev. Lett.* **2004**, *93*, 176806–4.
(33) Bondarev, I. V.; Slepyan, G. Y.; Maksimenko, S. A. *Phys. Rev. Lett.* **2002**, *89*, 115504–115504.

NL080048R